LANGMUIR

Article

pubs.acs.org/Langmuir

Comparative Study of Secondary Structure and Interactions of the R5 Peptide in Silicon Oxide and Titanium Oxide Coprecipitates Using Solid-State NMR Spectroscopy

Erika L. Buckle, Adrienne Roehrich, Branden Vandermoon, and Gary P. Drobny*

Department of Chemistry, University of Washington, Box 351700, Seattle, Washington 98195, United States

Supporting Information

ABSTRACT: A biomimetic, peptide-mediated approach to inorganic nanostructure formation is of great interest as an alternative to industrial production methods. To investigate the role of peptide structure on silica (SiO_2) and titania (TiO_2) morphologies, we use the R5 peptide domain derived from the silaffin protein to produce uniform SiO_2 and TiO_2 nanostructures from the precursor silicic acid and titanium bis(ammonium lactato)dihydroxide, respectively. The resulting biosilica and biotitania nanostructures are characterized using scanning electron microscopy. To investigate the process of R5-mediated SiO_2 and TiO_2 formation, we carry out 1D and 2D solid-state NMR (ssNMR) studies on R5 samples with uniformly ^{13}C- and ^{15}N-labeled residues to determine the backbone and side-chain chemical shifts. ^{13}C chemical shift data are in turn used to determine peptide backbone torsion angles and secondary structure for the R5 peptide neat, in silica, and in titania. We are thus able to assess the impact of the different mineral environments on peptide structure, and we can further elucidate from ^{13}C chemical shifts change the degree to which various side chains are in close proximity to the mineral phases. These comparisons add to the understanding of the role of R5 and its structure in both SiO_2 and TiO_2 formation.

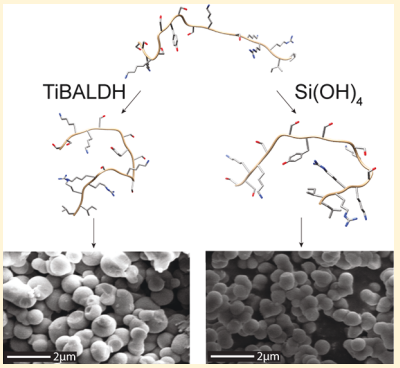

1. INTRODUCTION

Nanostructured silica (SiO_2) and titania (TiO_2) are versatile materials with widespread applications including use as pigments, insulators, textile coatings, catalysts, medical devices, and solar cell components.[1−10] Each specific application requires a uniquely tuned set of physical properties for the material, such as particle size, crystallinity, and morphology; thus, synthetic routes that allow for fine-tuned control are necessary.[11] However, despite the pervasive use of both SiO_2 and TiO_2 in the industrial and commercial sectors, production is not optimal; the anthropogenic synthesis often requires extreme temperature, pressure, and pH while maintaining limited control over crystallinity and morphology.[12−16]

In contrast, biological organisms produce inorganic materials through a process known as biomineralization. Diatoms, a unicellular microalgae, produce SiO_2 under mild conditions from the precursor silicic acid, resulting in material of tailored size and structure.[17−23] One of the most widely studied silicifying organisms is the marine diatom *Cylindrotheca fusiformis*. The protein implicated in regulating the process of SiO_2 biomineralization is silaffin sil1p. The primary structure of sil1p has a repetitive peptide sequence between residues 108 and 271, composed of seven units.[22] The fifth of these repeating units, a 19 amino acid peptide known as R5 (SSKKSGSYSGSKGSKRRIL), has the ability to precipitate SiO_2 nanospheres in a manner similar to its parent silaffin without the need for post-translational modifications.[22] Mutation studies by Knecht and Wright[22] have shown that R5 self-assembles to produce SiO_2 and that the C-terminal RRIL motif is integral to this process. The authors suggest that the RRIL motif encourages micellar self-assembly due to the arginine's guanidinium groups in close proximity to hydrophobic leucine and isoleucine residues.[22] Although this claim has been questioned recently by Senior et al.,[24] whose DLS study found no evidence of aggregate formation in solutions of R5, mutation studies by Lechner and Becker[25] support the need for the RRIL motif, however, not necessarily at the C-terminal position or in the native order. Lechner and Becker also demonstrated the importance of the amino groups of the lysine residues in SiO_2 formation. Their study found that the structure of the resulting SiO_2 is dependent on the number and position of lysine residues within the R5 sequence.[25] An alternative mechanism of R5-SiO_2 precipitation involves R5 self-assembly driven by salt bridges that form between the guanidine groups of arginine residues and phosphate anions. Cationic amino groups then bring silicic acid and SiO_2 particles into close proximity, which promotes the condensation reaction.[22,25] Additionally, peptides rich in lysine and various cationic polymers have been used to facilitate SiO_2 production with various morphologies.[26−29]

Biomimetic approaches are also being applied to the synthesis of nonbiological materials, specifically TiO_2, using

Received: March 27, 2017
Revised: August 22, 2017
Published: September 12, 2017

DOI: 10.1021/acs.langmuir.7b01048
Langmuir 2017, 33, 10517−10524

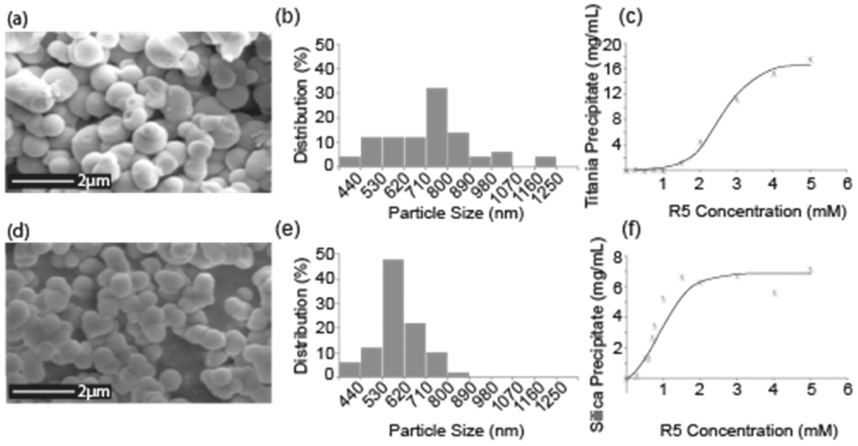

Figure 1. (a) SEM image of R5-TiO_2 coprecipitates showing spherical morphologies with a mean diameter of 734 ± 180 nm. (b) Size distribution histogram for R5-TiO_2 coprecipitates. Particle sizes are measured using ImageJ. (c) TiO_2 produced as a function of R5 concentration. The concentration of TiBALDH was held constant at 0.1 M. Data are a mean from two independent repeats. (d) SEM image of R5-SiO_2 coprecipitates showing spherical morphologies with a mean diameter of 596 ± 93 nm. (e) Size distribution histogram for R5-SiO_2 coprecipitates. Particle sizes are measured using ImageJ. (f) SiO_2 produced as a function of R5 concentration. The concentration of $Si(OH)_4$ was held constant at 0.1 M. Data are a mean from two independent repeats.

the precursor titanium bis(ammonium lactato)dihydroxide (TiBALDH).[30−37] An example of such an approach is that of Sewell and Wright,[37] who have shown that R5 can produce TiO_2 nanospheres under mild conditions when introduced into solutions containing TiBALDH.

Although much effort has been put forth to characterize the mechanism of R5's role in SiO_2 precipitation, significantly less work has been done to elucidate the role it plays in TiO_2 precipitation. Elucidating the structure of R5 within both SiO_2 and TiO_2 coprecipitates of similar morphology is an important first step in understanding how R5 directs the formation of TiO_2. By identifying the interactions of the amino acid residues of R5 with the surrounding SiO_2 or TiO_2 and the degree to which the structural principles that underlie the TiO_2-precipitating activity of R5 resemble or do not resemble the SiO_2-precipitating activity of R5, we can form comparisons between the two systems. By comparing the lesser-studied R5-TiO_2 to R5-SiO_2, we augment our understanding of the R5-TiO_2 system.

Here, we use solid-state ^{13}C NMR to characterize the structures of neat R5 (i.e., R5 lyophilized from Millipore water), R5 coprecipitated with TiO_2 (i.e., R5-TiO_2), and R5 coprecipitated with SiO_2 (i.e., R5-SiO_2) to obtain information on the structural changes that R5 undergoes within each mineral environment. We use chemical shift data and TALOS-N[38]-predicted torsion angles to determine the structures of the backbone for R5 neat, R5-SiO_2, and R5-TiO_2. We compare the structure of R5 within the TiO_2 coprecipitate to that within the SiO_2 coprecipitate, providing important insights into the behavior of R5 during mineral precipitation. The perturbation of side-chain ^{13}C chemical shifts is used to obtain information on the proximity of various amino acid side chains in R5 to the surrounding mineral as well as the role that various side chains might play in mineral precipitation. Finally, the conclusions drawn from our structural study of R5 in SiO_2 and TiO_2 coprecipitates are compared to several recent solid-state NMR studies of peptides and proteins in biosilica composites.

2. EXPERIMENTAL SECTION

2.1. Materials. All natural and uniformly labeled ^{13}C and ^{15}N amino acids were purchased from Sigma-Aldrich (St. Louis, MO). Preloaded Fmoc-protected Wang resin was purchased from EMD Millipore (Billerica, MA). All other reagents were purchased from Sigma-Aldrich (St. Louis, MO) and used without purification.

2.2. Peptide Synthesis. Peptides were synthesized on a CEM Liberty Blue peptide synthesizer using a standard 9-fluorenylmethoxycarbonyl (FMOC) and *tert*-butyl protection scheme. Preloaded Fmoc-protected Wang resin was used for solid-phase synthesis. Peptides were cleaved from the resin in a 10 mL solution of 95:2.5:2.5 trifluoroacetic acid/triisopropylsilane (TIS)/water per 1.0 g of peptide/resin. The resulting filtrate was added dropwise to cold *tert*-butyl methyl ether, followed by centrifugation and three rinses of the resulting solids with 40 mL of cold *tert*-butyl methyl ether. Peptides were purified using RP-HPLC (Varian ProStar HPLC, Alltima WP C4 column, 5 mL/min, eluent A consisting of water with 0.2% TFA, and eluent B consisting of acetonitrile with 0.2% TFA) with a gradient of 15−35% B over 40 min. Chromatograms were generated by observing the UV absorbance at 274 nm, and the analyte was verified by mass spectrometry. The fractions were then lyophilized, resulting in the pure peptide.

2.3. SiO_2 Precipitation. Orthosilicic acid ($Si(OH)_4$) was freshly made before each precipitation by dissolving 0.15 mL of tetramethyl orthosilicate in 0.85 mL of 1 mM HCl to form 1 M $Si(OH)_4$. Orthosilicic acid (100 μL per 5 mg R5) was added to a solution of R5 dissolved in phosphate−citrate buffer (1.00 mL, 100 mM, pH 7.0) and vortex mixed. The solution was incubated for 5 min at room temperature. The precipitated R5-SiO_2 was separated from the mixture via centrifugation at 15 000*g* for 10 min. The resulting precipitate was rinsed with Millipore water three times and dried in vacuo.

2.4. TiO_2 Precipitation. TiBALDH (100 μL per 5 mg R5, 1M) was added to a solution of R5 of varying concentrations dissolved in phosphate−citrate buffer (1.00 mL, 100 mM, pH 7.0) and vortex mixed. The solution was incubated for 30 min at room temperature. The precipitated R5-TiO_2 was separated from the mixture via centrifugation at 15 000*g* for 10 min. The resulting precipitate was rinsed with Millipore water three times and dried in vacuo.

2.5. SiO_2 and TiO_2 Morphology Characterization. SEM images were taken on a FEI Sirion XL30 scanning electron microscope operating at variable voltages. Precipitates were dispersed onto a carbon tap, mounted on aluminum studs, and sputter-coated for 60−90 s with Au/Pd.

2.6. Solid-State NMR. All solid-state NMR experiments were conducted using a 16.4 T magnetic field (proton resonant field of 700.18 MHz) on a Bruker Avance III spectrometer fitted with a ^1H {^{13}C,^{15}N} 3.2 mm MAS probe. The ^{13}C NMR signal was enhanced using cross-polarization (CP) with a $^1H-^{13}C$ contact time of 1.1 ms,

DOI: 10.1021/acs.langmuir.7b01048
Langmuir 2017, 33, 10517−10524

and a magic angle spinning (MAS) rate of 10−15 kHz ± 5 Hz was maintained with a Bruker MAS controller unit. One-dimensional ^{13}C CP-MAS experiments were performed with a proton 90° pulse time of 2.75 μs and a recycle delay of 2 s. The number of scans for the neat R5 and the R5-TiO_2 complex ranged from 2000 to 32 000. To obtain the resolution needed to confidently assign all of the chemical shifts in the R5 samples, 2D $^{13}C-^{13}C$ dipolar-assisted rotational resonance (DARR)[39] experiments were performed. The 2D spectra were collected with 30 or 60 ms mixing times and a recycle delay of 1.5 s, with 128 points in the indirectly detected dimension and 512 points in the directly detected dimension. All chemical shifts reported were indirectly referenced to tetramethylsilane (TMS) in the solid state using adamantane (δ = 38.48).[40]

3. RESULTS

3.1. Peptide-Mineral Precipitation. Figure 1 displays SEM images of the R5-TiO_2 (Figure 1a) and R5-SiO_2 (Figure 1d) coprecipitates. Both peptide−mineral coprecipitates are approximately spherical, but with varying average diameters consisting of an average diameter of 734 ± 180 nm for the R5-TiO_2 coprecipitates and 594 ± 93 nm for the R5-SiO_2 coprecipitates. The size distribution histograms for both the R5-TiO_2 coprecipitates (Figure 1b) and R5-SiO_2 coprecipitates (Figure 1e) are shown. The spherical morphologies of the R5-TiO_2 particles are consistent with those observed by Sewell and Wright,[37] although the average size of the R5-TiO_2 particles we observe is larger than what they report. The average size of the R5-SiO_2 particles we observe is consistent with those observed in the literature.[18,22,25]

Figure 1c,f illustrates the differences in R5 activity between the TiO_2 and SiO_2 systems. TiO_2 is precipitated only above 1 mM R5, whereas SiO_2 is precipitated above 0.5 mM R5. Although both systems are cooperative in nature based on the shape of the curves, it is more pronounced for the R5-TiO_2 system, suggesting that in order to induce TiO_2 formation, more R5 molecules must aggregate. This is consistent with the larger particle sizes seen for R5-TiO_2 coprecipitates (Figure 1b,e). There may also be significant electrostatic contributions to the larger amounts of SiO_2 precipitation at lower concentrations; the cationic R5 may have a stronger attraction to the more anionic SiO_2 than to TiO_2.[41] SiO_2 precipitation levels out at a much lower concentration of R5 than does TiO_2 precipitation, which also produces more product at the highest concentration tested.

Both R5-TiO_2 and R5-SiO_2 consist of R5 peptide that is embedded in a mineral nanostructure. Inductively coupled plasma optical emission spectrometry (Supporting Information Table S1) reveals that phosphorus is present in both mineral coprecipitates after extensive washing of the precipitated samples. The only source of phosphorus is phosphate anions present in the buffer, so logically it must be attributed to phosphate embedded within the coprecipitate, indicating an incorporation of the phosphate−citrate buffer within the coprecipitates. Examining the secondary structures of R5-TiO_2 and R5-SiO_2 can provide insight into how R5 interacts with the phosphates present in each mineral environment.

3.2. ^{13}C Chemical Shift Assignments for R5 Neat, R5-TiO_2, and R5-SiO_2 Peptide. ^{13}C chemical shift assignments for R5 neat, R5-TiO_2, and R5-SiO_2 are provided as Supporting Information (Tables S2−S7). To obtain site-specific chemical shift assignments, both one-dimensional ^{13}C CPMAS and two-dimensional (2D) dipolar-assisted rotational resonance (DARR) $^{13}C-^{13}C$ experiments were performed on R5-TiO_2. We were able to use DARR to resolve and assign most of the ^{13}C spectrum of R5 in TiO_2 containing up to three uniformly ^{13}C- and ^{15}N-enriched amino acids. To assign the chemical shifts for the entire peptide, seven isotopically enriched samples were analyzed, as shown in Table 1. The only amino acids not assigned by this study were S7, Y8, and C-terminal L19. Roehrich and Drobny[18] conducted the same set of experiments on the same seven enriched samples for both the neat R5 peptide and the R5-SiO_2 coprecipitate, to which comparisons will be made.[18]

Table 1. R5 Samples in Which Uniformly ^{13}C- and ^{15}N-Enriched Amino Acids Were Incorporated

sample name	label position
R5-S	S*SKKSGSYSGSKGSKRRIL
R5-SK	SS*K*KSGSYSGSKGSKRRIL
R5-KSG	SSKK*S*G*SYSGSKGSKRRIL
R5-GSKm	SSKKSGSYSG*S*K*GSKRRIL
R5-GSKc	SSKKSGSYSGSKG*S*K*RRIL
R5-R	SSKKSGSYSGSKGSKR*RIL
R5-SRI	SSKKSGSYS*GSKGSKRR*I*L

Figure 2 shows a typical DARR spectrum obtained from selectively ^{13}C-labeled peptide R5-GSKc TiO_2, which demonstrates the assignment of the ^{13}C spins in G13, S14, and K15. The horizontal and vertical lines delineate cross-peaks, which indicate networks of dipolar-coupled ^{13}C spins. To ensure the observation of only intraresidue cross-peaks, DARR spectra were taken with mixing times of 30 and 60 ms. In a few cases, however, unique chemical shifts could not be assigned; for example, it was not possible to assign the two $\delta^{13}C$ shifts for I18.

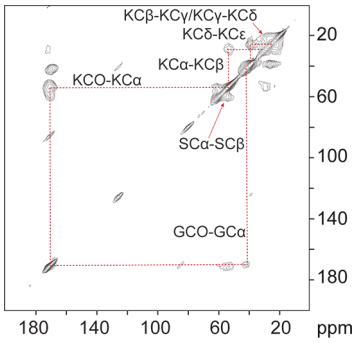

Figure 2. $^{13}C-^{13}C$ DARR spectrum for the R5-GSKc in the TiO_2 coprecipitate. Vertical and horizontal lines indicate assignments of ^{13}C spins in G13, S14, and K15.

Changes in the chemical shift (ΔCS) for backbone and side-chain ^{13}C nuclei in the neat versus coprecipitated samples occur to varying degrees at sites along the peptide backbone and side chains. The ^{13}C chemical shift perturbations of the backbone ^{13}CO, $^{13}C\alpha$, and $^{13}C\beta$ chemical shifts are associated with a change in secondary structure as a result of precipitation with SiO_2 or TiO_2. To study systematically the degree to which R5 peptide ^{13}C chemical shifts have been perturbed upon coprecipitation with SiO_2 and TiO_2, ΔCS values are obtained by subtracting the chemical shift of the ^{13}C spin in neat R5 from the corresponding ^{13}C spin in the R5-TiO_2 or R5-SiO_2 coprecipitate. A positive ΔCS indicates a downfield perturbation of the chemical shift (higher ppm, less shielded) in the coprecipitate versus in the neat solid peptide, and a negative

DOI: 10.1021/acs.langmuir.7b01048
Langmuir 2017, 33, 10517−10524

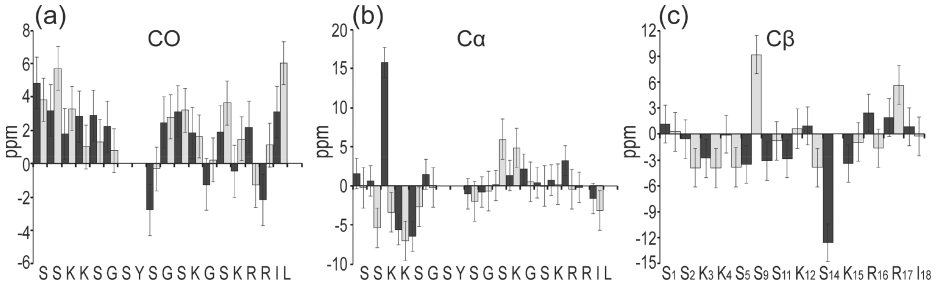

Figure 3. Backbone ΔCS plots showing chemical shift perturbations for (a) ^{13}CO shifts, (b) $^{13}C\alpha$ shifts, and (c) $^{13}C\beta$ shifts. ΔCS values for R5 coprecipitated with TiO_2 (black) and SiO_2 (gray) are in reference to the neat peptides. Positive changes indicate a downfield shift, and negative changes indicate an upfield shift relative to the neat peptide.

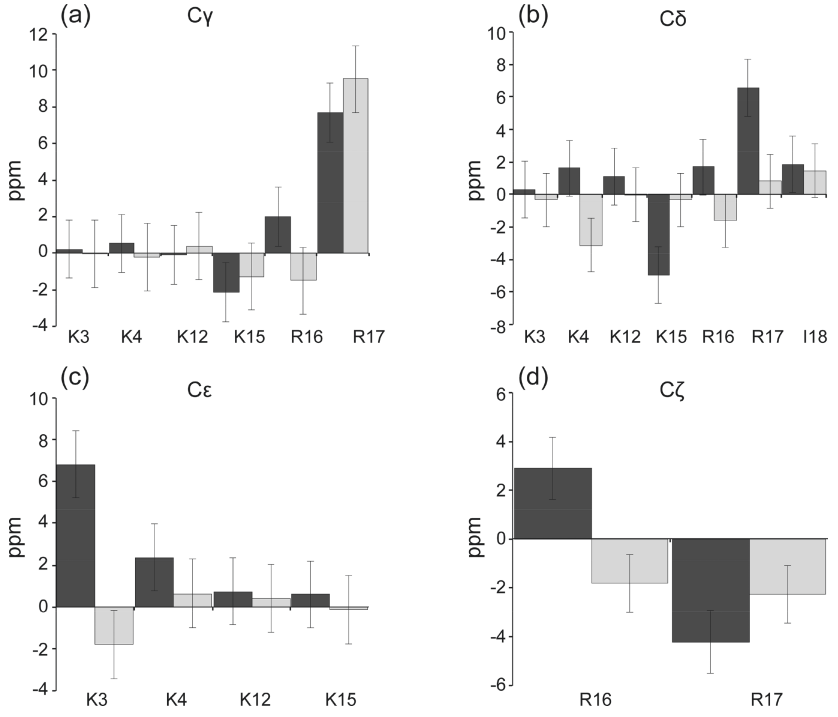

Figure 4. Side-chain ΔCS plots showing chemical shift perturbations for (a) $^{13}C\gamma$ shifts, (b) $^{13}C\delta$ shifts, (c) $^{13}C\varepsilon$ shifts, and (d) $^{13}C\zeta$ ΔCS for R5 coprecipitated with TiO_2 (black) and SiO_2 (gray) are in reference to the neat peptides. Positive changes indicate a downfield shift whereas negative changes indicate an upfield shift relative to the neat peptide.

ΔCS indicates an upfield perturbation of the chemical shift (lower ppm, more shielded). Bar charts of backbone ΔCS values are shown in Figure 3. In both R5-SiO_2 and R5-TiO_2, significant perturbations are observed in the S1, S2, and I18 ^{13}CO shifts, the K3, K4, and S5 $^{13}C\alpha$ shifts, and the S5, S14, and R17 $^{13}C\beta$ shifts. The chemical shift perturbations in R5-TiO_2 and R5-SiO_2 are similar for the S1 ^{13}CO, S2 ^{13}CO, and K4 $^{13}C\alpha$ shifts, indicating similar structural changes in R5 in both systems in these regions. The perturbations in I18 ^{13}CO, S5 $^{13}C\beta$, and R17 $^{13}C\beta$ are larger in magnitude for R5-SiO_2 than for R5-TiO_2, and the perturbations in K3 $^{13}C\alpha$ and S14 $^{13}C\beta$ are larger in magnitude in R5-TiO_2 than in R5-SiO_2.

Bar charts of side-chain ΔCS values are shown in Figure 4 for both the R5-SiO_2 and R5-TiO_2 systems. In R5-TiO_2, K3 ΔCS > 6 ppm for the $^{13}C\varepsilon$, and in R5-SiO_2, ΔCS values for $^{13}C\gamma$, $^{13}C\delta$, and $^{13}C\varepsilon$ range from 0 to −2 ppm. In previous ssNMR studies of polylysine adsorbed onto SiO_2,[42] an upfield perturbation of the lysine $^{13}C\varepsilon$ spin chemical shift was attributed to the proximity to the negatively charged SiO_2 surface. Downfield perturbation of the side-chain ^{13}C spin chemical shifts has been similarly interpreted as indicating proximity to positive charge centers in mineral surfaces.[42] Side-chain chemical shift trends in R5-SiO_2 and R5-TiO_2 suggest similar close associations between amino acid side chains and the inorganic oxide components. On the basis of these data, K3 is likely interacting with the mineral in both the SiO_2 and TiO_2 systems. In contrast, the $^{13}C\gamma$/$^{13}C\delta$/$^{13}C\varepsilon$ spins for K12 and K15 in R5-SiO_2 show much smaller or negligible ΔCS. However, we observe a significant upfield shift for $^{13}C\delta$ of K15 in R5-TiO_2, which is not present in R5-SiO_2.

As mentioned earlier, previous work has shown that the arginine residues in R5 are necessary for peptide self-assembly, either by the arginine side-chain's involvement with adjacent hydrophobic residues to effect micelle-like self-assembly[22] or by the formation of phosphate salt bridges between the arginine guanidinium groups.[25] The occurrence of guanidinium−phosphate interactions would be expected to perturb the electronic environment of the arginine side chains. Accordingly, significant chemical shift perturbations are observed in R5-SiO_2 and R5-TiO_2 for $^{13}C\gamma$, $^{13}C\delta$, and $^{13}C\zeta$ in R16 and R17.

DOI: 10.1021/acs.langmuir.7b01048
Langmuir 2017, 33, 10517−10524

3.3. Comparison of Local Peptide Structure in R5 Neat, R5-TiO_2, and R5-SiO_2. The chemical shifts obtained from the ^{13}CO, $^{13}C\alpha$, and $^{13}C\beta$ spins in neat R5, R5-TiO_2, and R5-SiO_2 DARR spectra were used to produce TALOS-N[38] input files. TALOS-N[38] output files consist of predicted torsion angles, which were used to visualize the changes in secondary structures for both R5 neat, R5-TiO_2, and R5-SiO_2 peptides using Chimera[43] (shown in Figure 5). Φ/Ψ torsion angle

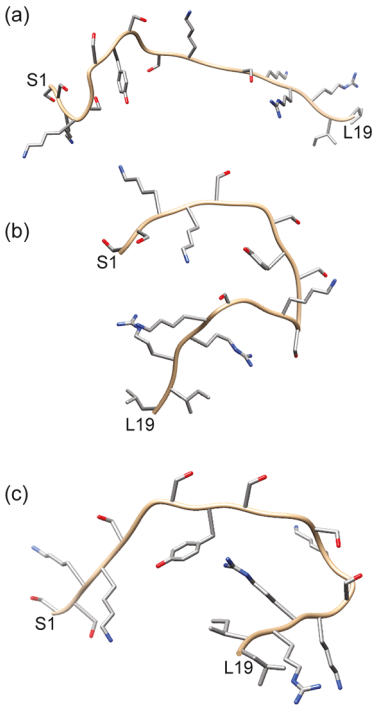

Figure 5. Chimera[43]-generated models of (a) R5 neat, (b) R5-TiO_2, and (c) R5-SiO_2 using TALOS-N[38]-generated torsion angles from experimentally obtained chemical shifts. The models are shown with Φ of −119 and Ψ of 113 (values consistent with the Φ/Ψ angles of surrounding residues and localized secondary structure) for the S7, Y8, and L19 positions because the backbone chemicals shifts for these residues were not determined in this study.

values for R5-SiO_2 and R5-TiO_2 generated by TALOS-N[38] are shown in the Supporting Information (Tables S8−S10). On the basis of the TALOS-N[38] analysis of ^{13}CO, $^{13}C\alpha$, and $^{13}C\beta$ chemical shifts, the majority of Φ torsion angles occur between −80 and −150° in the neat R5 peptide. Furthermore, the majority of Ψ torsion angles occur between 40 and 180°. Outliers occur at K4−S5 and near glycine residues G6-S7 and G10-S11. Aside from these amino acids, the majority of the peptide chain of the neat R5 peptide from S7 to I18 is in an extended conformation. The observed secondary structures for R5 in TiO_2 and SiO_2 are relatively similar and deviate from the neat structure in similar ways. In particular, R5 in SiO_2 and in TiO_2 both have significant changes in Φ values at the K3−K4 and K4−S5 positions. There is also a significant change in both Φ/Ψ at G13-S14. These differences in ΔCS values for R5 in SiO_2 composites versus R5 in TiO_2 composites can be discerned from so-called ΔΔCS maps, shown in Supporting Information Figure S8 for backbone ^{13}C chemical shifts and in Supporting Information Figure S9 for side-chain ^{13}C chemical shifts. In general, most of the aforementioned large torsion angle changes in R5-TiO_2 are matched by R5-SiO_2, with the exception of K3-K4, where the change in the Φ torsion angle in SiO_2 is not as large as in TiO_2. As a result of these torsion angle changes, both forms of mineral-associated R5 adopt extended structures of the N-terminal S2-K3-K4-S5 segment but deviate from an extended conformation in the G6-I18 region.

In both R5-SiO_2 and R5-TiO_2, perturbations in the backbone torsion angles near S2, K3, K4, and S5 are accompanied by a large ΔCS in the side chain of K3 and to a somewhat lesser extent in the side chain of K4 (Figure 4a−c). It is also interesting that the ΔCS for the $^{13}C\zeta$ spins in the side chains of R16 and R17 in R5-SiO_2 and R5-TiO_2 (Figure 4d) are also accompanied by structural changes of the backbone in the immediate vicinity of these residues but appear to be more modest than the structural changes that occur at and around K3 and K4. Although chemical shifts of side-chain ^{13}C spins beyond $^{13}C\beta$ are not correlated with protein secondary structure, a large ΔCS for these more distal sites reflects changes in the electronic environment associated with peptide precipitation with SiO_2 and TiO_2. Although we cannot quantify the origins of ΔCS for $^{13}C\gamma/^{13}C\delta/^{13}C\varepsilon/^{13}C\zeta$ spins to the degree that we can quantify ΔCS for $^{13}CO/^{13}C\alpha/^{13}C\beta$, we can combine our ΔCS results with data from other studies of peptide interactions with SiO_2 and TiO_2 to obtain insight into how R5 interacts with SiO_2 and TiO_2 precursors. This will be discussed further in the next section.

4. DISCUSSION

Solid-state NMR has been used extensively to study the structure and interactions of peptides in biosilica composites.[18,44−48] This is due in part to the occurrence of spin 1/2 nuclei in the peptide side chains and the occurrence of ^{29}Si, a spin 1/2 species with 4% natural abundance, in the mineral component, which together enable the study of peptide−silica interactions by solid-state NMR heteronuclear correlation methods. The interactions of peptides with nonbiological oxide TiO_2 are also of great interest, but an analogous solid-state NMR study of peptide TiO_2 interactions is complicated by the fact that recoupling to ^{47}Ti and ^{49}Ti nuclei is impractical. To circumvent this difficulty, in addition to a comparative chemical shift study of R5 secondary structure in SiO_2 versus TiO_2, we have also used ^{13}C chemical shifts to probe how the R5 peptide interacts with SiO_2 and TiO_2 in the respective R5 mineral composites as well as the degree to which the R5 peptide interacts with other components of the composite, including phosphate ions and other peptides.

The presence of spin 1/2 nucleus ^{29}Si in SiO_2 makes possible the direct determination of peptide−mineral contacts using heteronuclear NMR correlation methods, which in turn provides a means to interpret ΔCS trends directly for R5 in SiO_2 and to infer environmental origins for similar ΔCS trends for R5 in TiO_2. Several NMR studies have shown that molecules containing amine and/or amino groups make close contact with SiO_2 surfaces via these functional groups. Schmidt and co-workers[44] used $^{15}N\{^{29}Si\}$ REDOR to show that monomeric amino acids interact with SiO_2 surfaces via the NH_3^+ functional group. Brunner and co-workers[45] used $^1H-^{13}C-^{29}Si$ double-CP-based HETCOR NMR techniques to show that organic polyamines in biosilica from diatom species *Thalassiosira pseudonana* are closely associated with SiO_2. Recently, Goobes and co-workers[46] used $^1H-^{29}Si$ HETCOR experiments in combination with NMR signal enhancement via dynamic nuclear polarization (DNP) to show that lysine side-chain amine protons in the PL12 peptide (KAAKLFKPKASK) coprecipitated with SiO_2 are also in close

DOI: 10.1021/acs.langmuir.7b01048
Langmuir 2017, 33, 10517−10524

contact with SiO_2. Guo and Holland used $^1H-^{13}C$ HETCOR and ^{15}N and ^{13}C chemical shift data to establish that monomeric lysine binds to fumed silica primarily via the side-chain amine.[49] These NMR studies generally support the hypothesis that the ΔCS observed in the K3 and K4 side chains of R5 in SiO_2 originate from interactions between these side chains and the negatively charged SiO_2 surface. The general absence of significant ΔCS in the side chains of K12 and K15 in R5-SiO_2 in turn indicates the absence of interactions with SiO_2 at these sites. Furthermore, it is possible that the secondary structural rearrangements observed in the N-terminus of R5-SiO_2 coprecipitates occur to optimize contacts among K3, K4, and the adjacent SiO_2 interface.

Significant ΔCS trends are also observed for the $^{13}C\zeta$ spins of R16 and R17 in SiO_2. The upfield shift for the $^{13}C\zeta$ spins in the arginine guanidinium groups may be due to SiO_2 contacts, but the absence of similar contacts at the adjacent K15 argues against this scenario. The fact that R5 and other unmodified silaffin peptides will not precipitate SiO_2 in the absence of phosphate[50] and the apparent role played by arginine residues in R5 self-assembly via phosphate bridges[25] indicate that it is reasonable to assume that the upfield shifts we observe for the $^{13}C\zeta$ spins in R16 and R17 in R5-SiO_2 are due to interactions with phosphate ions.

The ΔCS map for R5-TiO_2 is somewhat more complicated to interpret than that of R5-SiO_2. Studies of peptide binding to oxidized titanium surfaces find that the surface oxide film consists of amorphous and nonstoichiometric TiO_2.[30,51] The surface hydroxyl groups in TiO_2 have pK_a's of 2.9 and 12.7 and thus at neutral pH exist as O^- and OH_2^+.[30,51,52] The fact that amorphous surface films of TiO_2 will accumulate both positively charged lysine[53] and negatively charged aspartate[54] supports the amphoteric nature of TiO_2. Accordingly, there are similarities and differences in the ΔCS maps for ^{13}C spins located at the distal positions of lysine and arginine side chains in R5-SiO_2 versus R5-TiO_2. As in R5-SiO_2, structural changes in the N-terminus of R5-TiO_2 correlate with the ΔCS in the K3 and K4 side chains, indicating that a secondary structural change may occur to optimize contacts between peptide side chains and TiO_2 precursors. Also, as in R5-SiO_2, the $^{13}C\zeta$ spins in the guanidinium groups of R16 and R17 in R5-TiO_2 display significant ΔCS but only modest structural changes.

There are some differences between the ΔCS observed for the $^{13}C\varepsilon$ lysine spins of K3 and K4 in R5-TiO_2 versus R5-SiO_2 that indicate differences in peptide−mineral interactions. For example, while $^{13}C\varepsilon$ of K3 shows a ΔCS of almost −2 ppm in SiO_2, the same spin has a ΔCS of +6 ppm in TiO_2. Downfield chemical shift changes observed for ^{13}C spins in peptides adsorbed onto inorganic surfaces have been attributed to the proximity to positive charge centers.[44] A possible explanation for the downfield shift observed for $^{13}C\varepsilon$ in TiO_2 is that the distal portion of the lysine side chain of K3 is laterally oriented relative to the TiO_2 surface, exposing the NH_3^+ group of the lysine side chain to an acidic hydroxyl group, whereas $^{13}C\varepsilon$ is oriented closer to a basic hydroxyl group or a Ti^{4+} ion. Although the hypothesis that R5 interacts with TiO_2 via lysine side chains is consistent, several recent STD NMR studies[55,56] of interactions between titanium binding peptide (i.e., TBP: RKLPDA) and TiO_2 nanocrystals, in the particular case of the $^{13}C\varepsilon$ of K3 in TiO_2 composites, indicate that the ΔCS interpretation is ambiguous. In R5, all lysine $^{13}C\varepsilon$ chemical shifts are close to 37 ppm, but the K3-$^{13}C\varepsilon$ chemical shift is close to 31 ppm. This value of the K3-$^{13}C\varepsilon$ chemical shift may indicate intra- or intermolecular interactions of this residue in the neat peptide that are disrupted upon coprecipitation with TiO_2. Therefore, whereas the upfield shift for K3-$^{13}C\varepsilon$ in silica likely indicates peptide−mineral interactions, the downfield shift for K3-$^{13}C\varepsilon$ in titania may be due to mineral−peptide interactions, changes in intra- or intermolecular interactions. or a combination of these effects.

The $^{13}C\zeta$ spins in R16 and R17 also have a more complicated ΔCS pattern in R5-TiO_2 than in R5-SiO_2. Unlike the R5-SiO_2 system, R5 will precipitate TiO_2 in the absence of phosphate, albeit at lower levels.[37] This raises the possibility that there are alternative mechanisms for the interaction of R5 with TiBALDH, and the upfield and downfield shifts observed for the $^{13}C\zeta$ spins in R16 and R17 may result from interactions between guanidinium groups and phosphate in addition to direct interactions with TiO_2 precursors. However, $^{13}C\gamma$ shifts of arginines are commonly in the region of 20−24 ppm, and whereas the $^{13}C\gamma$ of R16 falls in this range in the neat peptide, $^{13}C\gamma$ of R17 in the neat peptide is at 12.7 ppm and is shifted downfield by almost 8 ppm upon coprecipitation with TiO_2. Again, this may indicate the occurrence of some intra- or intermolecular interaction of the residue in the neat peptide, which is disrupted upon coprecipitation with TiO_2.

5. CONCLUSIONS

This is the first solid-state NMR study of the structure and interactions of silicifying peptide R5 in both a biosilica composite (i.e., R5-SiO_2) and a nonbiological metal oxide composite (i.e., R5-TiO_2). This study has produced site-specific chemical shift assignments for the majority of ^{13}CO, $^{13}C\alpha$, and $^{13}C\beta$ spins in the neat peptide and for the peptide in the two inorganic oxides, enabling a comparative study of R5 structure in all three environments. Numerous studies conclude that lysine residues in R5 are necessary for interactions with SiO_2/TiO_2 precursors. Thus, the curvatures induced in the peptide structures in the two mineral environments, which we derive from a TALOS-N[38] analysis of the ^{13}CO, $^{13}C\alpha$, and $^{13}C\beta$ chemical shifts, may function to maximize the exposure of the K3 and K4 side chains at the surface of the peptide aggregate to SiO_2/TiO_2 precursors.

This study has also acquired chemical shift assignments for the majority of the side-chain ^{13}C spins in neat R5 and for R5-SiO_2 and R5-TiO_2. The ΔCS trends for the lysine $^{13}C\varepsilon$ spins and the arginine $^{13}C\zeta$ spins in the R5-SiO_2 precipitate are interpreted using a model in which the N-terminal lysines are exposed at the surface of the peptide aggregate while the lysine $^{13}C\varepsilon$ spins closer to the C-terminus show smaller ΔCS, suggesting that K12 and K15 are removed from SiO_2 contacts with the arginine $^{13}C\zeta$ spins, which show ΔCS that most likely indicates contacts with phosphate anions. Whereas the secondary structure of R5 in TiO_2 resembles the structure of the peptide in SiO_2, ΔCS trends observed for lysine $^{13}C\varepsilon$ and arginine $^{13}C\zeta$ spins in R5-TiO_2 may be due to mineral−peptide interactions, interactions with phosphate ions, or possibly changes in intra- or intermolecular interactions upon precipitation with TiO_2.

■ ASSOCIATED CONTENT

Supporting Information

The Supporting Information is available free of charge on the ACS Publications website at DOI: 10.1021/acs.langmuir.7b01048.

DOI: 10.1021/acs.langmuir.7b01048
Langmuir 2017, 33, 10517−10524

CPMAS spectra of selected R5 peptides used in ^{13}C chemical shift assignments, figures showing differences between chemical shift perturbations for R5 in silica versus titania, percent composition of peptide−silica and peptide−titania composites, tabulated chemical shift assignments for backbone and side-chain ^{13}C spins, and backbone torsion angles generated by TALOS. (PDF)

AUTHOR INFORMATION

ORCID

Gary P. Drobny: 0000-0002-7293-1897

Notes

The authors declare no competing financial interest.

ACKNOWLEDGMENTS

Part of this work was conducted at the Molecular Analysis Facility, which is supported in part by funds from the Molecular Engineering & Sciences Institute, the Clean Energy Institute, and the National Science Foundation (grant CHE-1219509). G.P.D. acknowledges National Institutes of Health grant RO1-GM109417, support from subcontract ANSK-0119-16, and helpful conversations with Professor Havard Haugen of the Department of Biomaterials, Institute for Clinical Chemistry University of Oslo, and with Dr. Martin Drazinzky, Institute for Organic Chemistry and Biochemistry, Prague, Czech Republic.

REFERENCES

(1) Fujishima, A.; Honda, K. *Nature* **1972**, *238*, 37−38.
(2) Hoffmann, M. R.; Martin, S. T.; Choi, W.; Bahnemannt, D. W.; Keck, W. M. *Chem. Rev.* **1995**, *95*, 69−96.
(3) Linsebigler, A. L.; Lu, G.; Yates, J. T. J. *Chem. Rev.* **1995**, *95*, 735−758.
(4) Abo-Farha, S. A. *The Journal of American Science* **2010**, *6* (611), 130−142, DOI: 10.7537/marsjas061110.18.
(5) Li, G.; Gray, K. A. *Chem. Phys.* **2007**, *339*, 173−187.
(6) Adachi, M.; Murata, Y.; Wang, F.; Jiu, J. In *Self-Organized Nanoscale Materials*; Springer: New York, 2006; pp 71−100.
(7) Acevedo, A.; Carpio, E. A.; Rodríguez, J.; Manzano, M. A. Disinfection of Natural Water by Solar Photocatalysis Using Immobilized TiO2 Devices: Efficiency in Eliminating Indicator Bacteria and Operating Life of the System. *J. Sol. Energy Eng.* **2012**, *134* (1), 011008.
(8) Varghese, O. K.; Grimes, C. A. *J. Nanosci. Nanotechnol.* **2003**, *3*, 277−293.
(9) Wintermantel, E.; Eckert, K.-L.; Huang, N.-P.; Textor, M.; Brunette, D. M. Springer: Berlin, 2001, 649−671.
(10) Chen, X.; Mao, S. S. *Chem. Rev.* **2007**, *107*, 2891−2959.
(11) Zhang, Z.; Wang, C.-C.; Zakaria, R.; Ying, J. Y. *J. Phys. Chem. B* **1998**, *102*, 10871−10878.
(12) Qian, Y.; Chen, Q.; Chen, Z.; Fanb, C.; Zhou, G. *J. Mater. Chem.* **1993**, *3* (2), 203−205.
(13) Chhabra, V.; Pillai, V.; Mishra, B. K.; Morrone, A.; Shah, D. 0. *Langmuir* **1995**, *11*, 3307−3311.
(14) Cheng, H.; Ma, J.; Zhao, Z.; Qi, L. *Chem. Mater.* **1995**, *7*, 663−671.
(15) Jang, H. D.; Kim, S.-K. *Mater. Res. Bull.* **2001**, *36*, 627−637.
(16) Wang, C.-C.; Ying, J. Y. *Chem. Mater.* **1999**, *11*, 3113−3120.
(17) Mann, S.; Archibald, D. D.; Didymus, J. M.; Douglas, T.; Heywood, B. R.; Meldrum, F. C.; Reeves, N. J. *Science* **1993**, *261* (5126), 1286.
(18) Roehrich, A.; Drobny, G. P. *Acc. Chem. Res.* **2013**, *46* (9), 2136−2144.
(19) Belton, D. J.; Patwardhan, S. V.; Perry, C. C. *J. Mater. Chem.* **2005**, *15*, 4629−4638.
(20) Kröger, N.; Deutzmann, R.; Sumper, M. *Science (Washington, DC, U. S.)* **1999**, *286* (5442), 1129−1132.
(21) Kröger, N.; Deutzmann, R.; Bergsdorf, C.; Sumper, M. *Proc. Natl. Acad. Sci. U. S. A.* **2000**, *97* (26), 14133−14138.
(22) Knecht, M. R.; Wright, D. W. *Chem. Commun.* **2003**, *24*, 3038.
(23) Lopez, P.; Gautier, C.; Livage, J.; Coradin, T. *Curr. Nanosci.* **2005**, *1* (1), 73−83.
(24) Senior, L.; Crump, M. P.; Williams, C.; Booth, P. J.; Mann, S.; Perriman, A. W.; Curnow, P. *J. Mater. Chem. B* **2015**, *3* (13), 2607−2614.
(25) Lechner, C. C.; Becker, C. F. W. *J. Pept. Sci.* **2014**, *20* (2), 152−158.
(26) Belton, D.; Paine, G.; Patwardhan, S. V.; Perry, C. C. *J. Mater. Chem.* **2004**, *14*, 2231−2241.
(27) Rodríguez, F.; Glawe, D. D.; Naik, R. R.; Hallinan, K. P.; Stone, M. O. *Biomacromolecules* **2004**, *5*, 261−265.
(28) Sumper, M.; Lorenz, S.; Brunner, E. *Angew. Chem., Int. Ed.* **2003**, *42* (42), 5192−5195.
(29) Deming, T. J.; Cha, J. N.; Stucky, G. D.; Morse, D. E. *Nature* **2000**, *403* (6767), 289−292.
(30) Sano, K.-I.; Sasaki, H.; Shiba, K. *Langmuir* **2005**, *21*, 3090−3095.
(31) Cole, K. E.; Valentine, A. M. *Biomacromolecules* **2007**, *8*, 1641−1647.
(32) Durupthy, O.; Bill, J.; Aldinger, F. *Cryst. Growth Des.* **2007**, *7* (12), 2696−2704.
(33) Dickerson, M. B.; Jones, S. E.; Cai, Y.; Ahmad, G.; Naik, R. R.; Kröger, N.; Sandhage, K. H. *Chem. Mater.* **2008**, *20*, 1578−1584.
(34) Kharlampieva, E.; Min Jung, C.; Kozlovskaya, V.; Tsukruk, V. V. *J. Mater. Chem.* **2010**, *20*, 5242−5250.
(35) Hernández-Gordillo, A.; Hernández-Arana, A.; Campero, A.; Vera-Robles, L. I. *Langmuir* **2014**, *30* (14), 4084−4093.
(36) Puddu, V.; Slocik, J. M.; Naik, R. R.; Perry, C. C. *Langmuir* **2013**, *29* (30), 9464−9472.
(37) Sewell, S. L.; Wright, D. W. *Chem. Mater.* **2006**, *18* (13), 3108−3113.
(38) Shen, Y.; Bax, A. *J. Biomol. NMR* **2013**, *56* (3), 227−241.
(39) Takegoshi, K.; Nakamura, S.; Terao, T. *Chem. Phys. Lett.* **2001**, *344* (5−6), 631−637.
(40) Morcombe, C. R.; Zilm, K. W. *J. Magn. Reson.* **2003**, *162* (2), 479−486.
(41) Patwardhan, S. V.; Emami, F. S.; Berry, R. J.; Jones, S. E.; Naik, R. R.; Deschaume, O.; Heinz, H.; Perry, C. C. *J. Am. Chem. Soc.* **2012**, *134* (14), 6244−6256.
(42) Fernandez, V. L.; Reimer, J. A.; Denn, M. M. *J. Am. Chem. Soc.* **1992**, *114*, 9634−9642.
(43) Pettersen, E. F.; Goddard, T. D.; Huang, C. C.; Couch, G. S.; Greenblatt, D. M.; Meng, E. C.; Ferrin, T. E. *J. Comput. Chem.* **2004**, *25* (13), 1605−1612.
(44) Ben Shir, I.; Kababya, S.; Amitay-Rosen, T.; Balazs, Y. S.; Schmidt, A. *J. Phys. Chem. B* **2010**, *114*, 5989−5996.
(45) Wisser, D.; Bruckner, S. I.; Wisser, F. M.; Althoff-Ospelt, G.; Getzschmann, J.; Kaskel, S.; Brunner, E. *Solid State Nucl. Magn. Reson.* **2015**, *66−67*, 33−39.
(46) Geiger, Y.; Gottlieb, H. E.; Akbey, Ü.; Oschkinat, H.; Goobes, G. *J. Am. Chem. Soc.* **2016**, *138* (17), 5561−5567.
(47) Zane, A. C.; Michelet, C.; Roehrich, A.; Emani, P. S.; Drobny, G. P. *Langmuir* **2014**, *30* (24), 7152−7161.
(48) Schug, K. A.; Lindner, W. *Chem. Rev.* **2005**, *105* (1), 67−114.
(49) Guo, C.; Holland, G. P. *J. Phys. Chem. C* **2014**, *118*, 25792−25801.
(50) Kroger, N. *Science (Washington, DC, U. S.)* **2002**, *298* (5593), 584−586.
(51) Sano, K.-I.; Shiba, K. *J. Am. Chem. Soc.* **2003**, *125*, 14234−14235.
(52) Hayashi, T.; Sano, K.-I.; Shiba, K.; Iwahori, K.; Yamashita, I.; Hara, M. *Langmuir* **2009**, *25* (18), 10901−10906.
(53) Roddick-Lanzilotta, A. D.; Connor, P. A.; Mcquillan, A. J. *Langmuir* **1998**, *14*, 6479−6484.

DOI: 10.1021/acs.langmuir.7b01048
Langmuir 2017, 33, 10517−10524

(54) Roddick-Lanzilotta, A.; McQuillan, A. *J. Colloid Interface Sci.* **2000**, *227* (1), 48−54.
(55) Mirau, P. A.; Naik, R. R.; Gehring, P. *J. Am. Chem. Soc.* **2011**, *133*, 18243−18248.
(56) Suzuki, Y.; Shindo, H.; Asakura, T. *J. Phys. Chem. B* **2016**, *120* (20), 4600−7.

DOI: 10.1021/acs.langmuir.7b01048
Langmuir 2017, 33, 10517−10524